DOI: 10.1002/chem.200600258

Valence Tautomerism in Octahedral and Square-Planar Phenoxyl–Nickel(II) Complexes: Are Imino Nitrogen Atoms Good Friends?

Olaf Rotthaus,[a] Fabrice Thomas,*[a] Olivier Jarjayes,*[a] Christian Philouze,[a] Eric Saint-Aman,[b] and Jean-Louis Pierre[a]

Abstract: The two tetradentate ligands H_2L and H_2L^{Me} afford the slightly distorted square-planar low-spin Ni^{II} complexes **1** and **2**, which comprise two coordinated phenolate groups. Complex **1** has been electrochemically oxidized into $\mathbf{1}^+$, which contains a coordinated phenoxyl radical, with a contribution from the nickel orbital. In the presence of pyridine, $\mathbf{1}^+$ is converted into $\mathbf{1_{Py}}^+$, an octahedral phenolate nickel(III) complex with two pyridines axially coordinated: An intramolecular electron transfer (valence tautomerism) is promoted by the geometrical changes, from square planar to octahedral, around the metal center. The tetradentate ligand H_2L^{Me}, in the presence of pyridine, and the hexadentate ligand H_2L^{Py} in CH_2Cl_2 afford, respectively, the octahedral high-spin Ni^{II} complexes $\mathbf{2_{Py}}$ and **3**, which involve two equatorial phenolates and two axially coordinated pyridines. At 100 K, the one-electron-oxidized product $\mathbf{2_{Py}}^+$ comprises a phenoxyl radical ferromagnetically coupled to the high-spin Ni^{II} ion, with large zero-field splitting parameters, while $\mathbf{3}^+$ involves a phenoxyl radical antiferromagnetically coupled to the high-spin Ni^{II} ion.

Keywords: hybridization · nickel · radicals · Schiff bases · valence tautomerism

Introduction

A growing number of metalloproteins are believed to use free radicals as cofactors to promote oxidation reactions.[1] A prototypical enzyme of this class is galactose oxidase (GO): Its active site harbors a tyrosyl radical (Tyr272$^{\bullet}$) coordinated, and antiferromagnetically exchange coupled, to a copper(II) atom.[2] GO catalyzes the two-electron oxidation of alcohols into aldehydes, with concommitent reduction of dioxygen into hydrogen peroxide. It represents a fascinating example of cooperativity between a metal and a radical to perform oxidation reactions: The copper(II) ion binds the substrate by its hydroxy group, thus favoring its deprotonation. The energy of the C_α–H bond to be broken is then lowered, thereby making hydrogen abstraction by the organic radical (stabilized by metal coordination) easier.

To model the active site of GO, several biomimetic approaches have been developed during the last decade. Consequently, a large number of complexes of the first-row transition metals with noninnocent ligands, especially copper(II)–phenoxyl complexes,[3–5] have been synthesized. In slightly distorted square-planar Ni^{II} complexes, the energy levels of the potentially redox-active orbitals, that is, π orbitals from the ligand or d orbitals from the metal, are very similar: By shifting one above the other, a metal-based or a ligand-based redox process could be favored. Ni^{II}–semiquinonate (or –iminosemiquinonate) complexes,[6] and more recently Ni^{II}–semicarbazide and some Ni^{II}–π-radicals,[7] have been reported. Only a few Ni^{II}–phenoxyl complexes have been described.[8–11] We have recently shown, in low-spin Ni^{II} complexes of salen-type prophenoxyl ligands (involving imino or amidato N donors), that the ligand field dramatically affects the oxidation locus.[9] We observed the following rule when exogenous pyridine was added to the medium: Electrochemical oxidation of Ni^{II}–phenolate complexes affords octahedral Ni^{III}–phenolate species ($S = {}^1/_2$), in which the metal is axially ligated by two pyridine molecules.[9] Previously, Wieghardt and co-workers have demonstrated that oxidation of the octahedral Ni^{II}–phenolate complexes $[Ni^{II}(L^4)(Ph_2acac)]^-$ and $[Ni^{II}(L^1)(Ph_2acac)]^-$ (L = ligand, acac = ace-

[a] Dr. O. Rotthaus, Dr. F. Thomas, Dr. O. Jarjayes, Dr. C. Philouze, Prof. Dr. J.-L. Pierre
Laboratoire de Chimie Biomimétique
LEDSS, UMR CNRS 5616, Université J. Fourier
BP 53, 38041, Grenoble cedex 9 (France)
Fax: (+33) 4-7651-4836
E-mail: Fabrice.Thomas@ujf-grenoble.fr
Olivier.Jarjayes@ujf-grenoble.fr.

[b] Prof. Dr. E. Saint-Aman
LEOPR, UMR CNRS 5630, Université J. Fourier
BP 53, 38041 Grenoble Cedex 9 (France).

tylacetonate) affords Ni^{II}–phenoxyl species, in which the radical is ferromagnetically coupled to a high-spin Ni^{II} center ($S_{total}=3/2$),[10] while Yamauchi and co-workers have reported that oxidation of pentacoordinated Ni^{II}–phenolate complexes affords Ni^{II}–phenoxyl species in which the radical is antiferromagnetically coupled to a high-spin Ni^{II} center ($S_{total}=1/2$).[11]

In the present paper, we investigate the effect of the ligand denticity and field on the oxidation locus in Ni^{II} complexes with three salen-type prophenoxyl ligands, namely, H_2L, H_2L^{Me}, and H_2L^{Py} (Scheme 1). H_2L possesses two salicylidene moieties connected together by an ethylidene spacer. H_2L^{Me} differs from H_2L in its coordinating nitrogen atoms, which are methylamino groups instead of the imines in H_2L. H_2L and H_2L^{Me} are designed to coordinate the metal cation in a tetradentate fashion. The two methylamino groups of H_2L^{Me} are replaced by (methylpyridine)amino arms in H_2L^{Py}, thereby making H_2L^{Py} a potentially hexadentate ligand, unlike H_2L and H_2L^{Me}. The structure, spectroscopic properties, spin configuration, and oxidative behavior of the Ni^{II} complexes are presented herein.

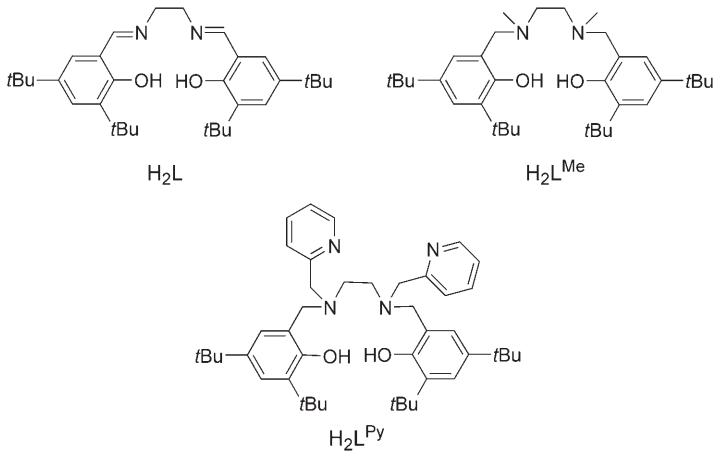

Scheme 1. Ligands used in this study.

Results and Discussion

Preparation of the ligands and complexes: The ligands H_2L,[5] H_2L^{Me},[12] and H_2L^{Py}[13] have been previously described. The tetradentate ligands H_2L and H_2L^{Me} provide an N_2O_2 coordination sphere for a single metal ion. H_2L^{Py} is a hexadentate ligand with a N_4O_2 donor set. Complex **1** was obtained by adding one molar equivalent of $Ni(ClO_4)_2\cdot 6H_2O$ to H_2L in the presence of two molar equivalents of NEt_3. Upon mixing $Ni(OAc)_2\cdot 4H_2O$ with the ligand H_2L^{Me} or H_2L^{Py} in methanol in the presence of two equivalents of NEt_3, the Ni^{II} complexes **2** and **3**, respectively, were obtained.

Structures of the Ni^{II} complexes: The crystallographic data for **2** and **3** are reported in Table 1 and selected bond lengths and angles are listed in Table 2.

Table 1. Crystallographic data for **2** and **3**.

	2	**3**
formula	$C_{34}H_{54}NiN_2O_2$	$C_{23.75}H_{37}Ni_{0.5}N_2O_{2.75}$
M	581.51	423.92
crystal system	orthorhombic	monoclinic
space group	*Pbca*	*C*2/*c*
a [Å]	17.404(2)	16.652(6)
b [Å]	10.906(2)	15.075(5)
c [Å]	34.480(3)	18.581(7)
α [°]	89	90
β [°]	89	90.81(2)
γ [°]	90	90
V [Å^3]	6544(1)	4664(3)
Z	8	8
T [K]	150	150
ρ_{calcd} [g cm^{-3}]	1.180	1.223
μ [cm^{-1}]	6.23	4.65
monochromator	graphite	graphite
wavelength	$Mo_{K\alpha}$ (0.71073 Å)	MoKα (0.71073 Å)
reflections collected	70026	38607
independent reflections (R_{int})	6386 (0.16441)	6806 (0.10953)
observed reflections	2874 [$I>2\sigma(I)$]	4895 [$I>2\sigma(I)$]
R	0.0408	0.0446
R_w	0.0553	0.0714

Table 2. Selected bond lengths [Å] and angles [°] for **2** and **3**.

2		
Ni–O1 1.848(2)	Ni–O2 1.860(2)	Ni–N1 1.937(3)
Ni–N2 1.932(3)		
O1-Ni-N1 93.7(1)	O2-Ni-N2 93.0(1)	O1-Ni-O2 85.7(1)
N1-Ni-N2 88.6(1)	O1-Ni-N2 171.3(1)	O2-Ni-N1 172.9(1)
3		
Ni–O1 1.974(1)	Ni–N1 2.133(1)	Ni–N2 2.118(1)
O1-Ni-O1 93.31(7)	O1-Ni-N1 91.48(5)	O1-Ni-N1 169.55(5)
O1-Ni-N2 95.15(5)	O1-Ni-N2 90.83(5)	N1-Ni-N1 85.37(7)
N1-Ni-N2 79.48(5)	N2-Ni-N2 94.07(5)	N2-Ni-N2 171.29(7)

The X-ray crystal structure of **2** is shown in Figure 1. The metal ion is coordinated to two phenolate oxygen atoms (O1, O2) and two amine nitrogen atoms (N1, N2). The geometry around the nickel atom is square planar distorted toward tetrahedral: The bond lengths Ni–O1 and Ni–O2 (1.848(2) and 1.860(2) Å, respectively) are shorter than the Ni–N1 and Ni–N2 lengths (1.937(3) and 1.932(3) Å, respectively). The angles for O1-Ni-O2, O1-Ni-N1, O2-Ni-N2, and N1-Ni-N2 differ slightly from 90° (85.7(1)°, 93.7(1)°, 93.0(1)°, and 88.6(1)°, respectively), while the O1-Ni-N2 and O2-Ni-N1 angles are 171.3(1)° and 172.9(1)°, respectively. The mean deviation from the least-square plane defined by the N1, N2, O1, O2, and Ni atoms is 0.1033 Å, with the nitrogen atoms N1 and N2 being displaced by −0.1352 and 0.1529 Å, respectively, from this plane. The dihedral angle between the two O-Ni-N planes is 169.3°. The torsion angle around the N1-C8-C9-N2 bridge is 50.2(3)°, with the C8 and

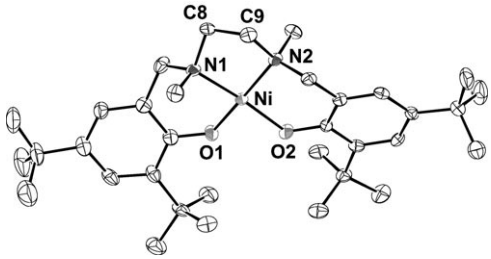

Figure 1. X-ray crystal structure of **2**, shown with 30% thermal ellipsoids (hydrogen atoms are omitted for clarity).

C9 atoms displaced −0.3777 and 0.2906 Å, respectively, from the N1-N2-Ni plane.

The ORTEP view of **3** is depicted in Figure 2. The coordination sphere of the nickel atom is best described as a distorted octahedron. The two halves of **3** have the same geometry and are related by an inversion center at the nickel atom. The two phenolate oxygen atoms (O1, O1*) and the two amine nitrogen atoms (N1, N1*) coordinate in a *cis* configuration to the equatorial plane. The bond lengths Ni–O1* and Ni–N1* are 1.974(1) and 2.133(1) Å, respectively. These bonds are much longer than the corresponding ones in **2**, a fact indicating that the spin state of the metal center is different in these complexes, that is, it is low spin in **2** and high spin in **3**. The pyridine nitrogen atoms coordinate in a *trans* configuration with an Ni–N2 bond length of 2.118(1) Å. The dihedral angle between the O1-Ni-N1 and O1*-Ni-N1* planes is close to that obtained for **2** (166.5°), as is the torsion angle around the N1-C8-C8*-N1* ethylene bridge (−59.7(2)°) and the mean deviation from the least-square plane defined by the N1, N1*, O1, O1*, and Ni atoms (0.1383 Å). The N1 and N1* atoms are displaced by 0.1723 and −0.1723 Å, respectively, from this latter plane, while the C8 and C8* atoms are displaced by −0.3619 and 0.3619 Å, respectively, on opposite sides of the N1-Ni-N1* plane.

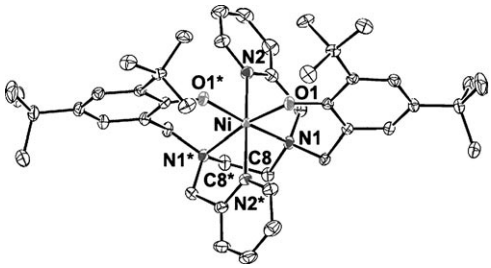

Figure 2. X-ray crystal structure of **3**, shown with 30% thermal ellipsoids (hydrogen atoms are omitted for clarity).

Interestingly, Neves et al. have recently reported the X-ray crystal structure of a zinc complex of H_2L^{Py}, prepared from $Zn(OAc)_2{\cdot}2H_2O$, in the absence of any base other than acetate.[12] Only one phenol of the ligand is deprotonated and the structural arrangement around the metal center is clearly different than that in **3**: The geometry around the zinc ion is distorted square pyramidal, with two pyridine nitrogen atoms, one tertiary amine nitrogen atom, and one phenolate oxygen atom occupying the basal plane. The remaining tertiary amine nitrogen atom coordinates in the apical position, while the other phenol oxygen atom is not coordinated to the zinc(II) ion. Full deprotonation of the H_2L^{Py} ligand is achieved in **3** by using an exogenous base that is stronger than acetate (NEt_3) and by the stronger Lewis acid character of the Ni^{II} ion compared to that of zinc(II).

Spectroscopic properties of the Ni^{II} complexes: Complexes **1**–**3** are X-band EPR silent at 100 K. However, **1** and **2** only show their ^1H NMR signals (in $CDCl_3$) within the diamagnetic region. **3** exhibits NMR signals over an 80-ppm spectral width, thereby showing that it is paramagnetic, in spite of its "X-band EPR silence". Such behavior is not unexpected: At the conventional frequency of 9.4 GHz (X-band), the microwave quantum energy is approximately 0.3 cm^{-1}. In transition metal ions with integer-spin ground state, the magnitude of the axial zero-field splitting parameter $|D|$ is often larger than this quantum and no EPR spectrum can be detected.[14]

Complexes **1** and **2** are thus diamagnetic low-spin Ni^{II} complexes, while **3** is a high-spin Ni^{II} species. The difference in spin state between **2** and **3** is interpreted by pyridine axial ligation in **3** affording an octahedral complex and thus inducing a high-spin configuration.

The UV/Vis spectrum of **1** in CH_2Cl_2 (Figure 3, Table 3) is dominated by intense absorptions at 349 ($\varepsilon = 9180$) and

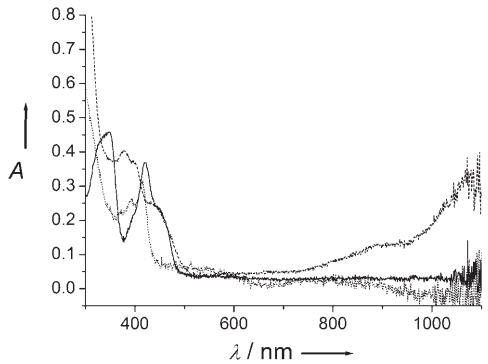

Figure 3. Electronic spectra of 0.05 mM solutions of **1** (solid lines), the electrogenerated $\mathbf{1}^+$ (dashed lines), and $\mathbf{1}^{2+}$ (dotted lines, recalculated spectrum) in CH_2Cl_2 containing 0.005 M TBAP. $T = 233$ K, path length = 1.000 cm. TBAP = tetra-*n*-butylammonium perchlorate.

422 nm (7380 $M^{-1}cm^{-1}$), a shoulder at 449 nm ($\varepsilon =$ 4740 $M^{-1}cm^{-1}$), and a broad lower intensity transition at 560 nm ($\varepsilon = 720$ $M^{-1}cm^{-1}$). The 422-nm band corresponds to charge-transfer (CT) transitions: It is red shifted and less intense than the CT transition of the previously described analogous copper(II) complex ($\lambda_{max} = 405$ nm ($\varepsilon =$ 11 440 $M^{-1}cm^{-1}$)).[5,15] The shorter wavelength features are associated with π–π* transitions, while the longer wave-

Table 3. Electronic properties of the nickel complexes in CH_2Cl_2 solution.

Complex	λ_{max} [nm][a] (ε [$M^{-1}cm^{-1}$])
1	349 (9180), 422 (7380), 449 sh (4740), 560 (720)
$\mathbf{1}^+$	300 (18720), 379 (8060), 399 (7340), 436 sh (4920), 899 br (2560), 1090 br (6980)[b]
$\mathbf{1}_{Py}{}^+$	337 (12140), 429 (7280), 493 (8140)[b]
$\mathbf{1}^{2+}$	395 (5260), 414 (6230), 550 br (1000)[b,c]
2	311 sh (10540), 377 (2320), 522 (1960)
$\mathbf{2}^{2+}$	390 (5740), 406 (7700), 530 br (1960)[b]
$\mathbf{2}_{Py}$	305 (21000), 310 sh (20400), 381 (1400), 526 (300)[b]
$\mathbf{2}_{Py}{}^+$	393 (2800), 412 (3300), 665 br (900)[b]
$\mathbf{2}_{Py}{}^{2+}$	397 (5700), 411 (7300), 540 br (1580)[b]
3	310 (13500), 369 sh (760), 610 (46)[b]
$\mathbf{3}^+$	391 (3160), 405 (3140), 611 br (2160)[b]
$\mathbf{3}^{2+}$	302 (22920), 391 (6400), 408 (8240), 528 (3460)[b]

[a] sh = shoulder, br = broad. [b] UV/Vis spectra recorded at 238 K in the presence of 0.005 M TBAP (CH_2Cl_2 + 0.1 M TBAP solutions electrochemically oxidized and diluted twenty-times). [c] Reconstituted spectrum: see the text.

length bands correspond to the d–d transitions of a d^8 low-spin Ni^{II} center in a slightly distorted square-planar geometry. The electronic spectrum of **2** in CH_2Cl_2 (Figure 4, Table 3) exhibits absorptions at 311 ($\varepsilon = 10540$), 377 (2320), and 522 nm (1960 $M^{-1}cm^{-1}$). Compared to **1**, the CT band is blue shifted while the d–d transition is red shifted.

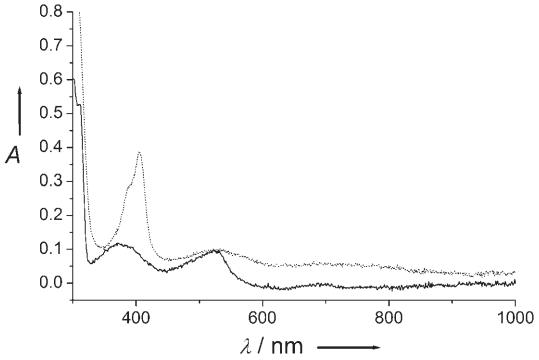

Figure 4. Electronic spectra of 0.05 mM solutions of **2** (solid lines) and the electrogenerated $\mathbf{2}^{2+}$ (dotted lines) in CH_2Cl_2 containing 0.005 M TBAP. $T = 233$ K, path length = 1.000 cm.

The electronic spectrum of **3** (Figure 5, Table 3) is quite different than that of **1** or **2**, as no absorption band with intensity $> 100\ M^{-1}cm^{-1}$ could be detected above 400 nm. The spectrum consists of transitions at 310 nm ($\varepsilon = 13500\ M^{-1}cm^{-1}$) and a shoulder at 369 nm ($\varepsilon = 760\ M^{-1}cm^{-1}$). The very weak d–d transition observed at 610 nm ($\varepsilon = 46\ M^{-1}cm^{-1}$) is characteristic of a d^8 high-spin Ni^{II} center in an octahedral geometry (spin-allowed $^3A_{2g} \rightarrow {}^3T_{1g}$ transition).[16]

Increasing amounts of pyridine were added to CH_2Cl_2 solutions of **1**–**3** at 298 K. Upon addition, no significant changes occur in the UV/Vis spectra of **1** and **3**. This shows that either the binding constant is very low or the metal electronic configuration is retained upon binding.

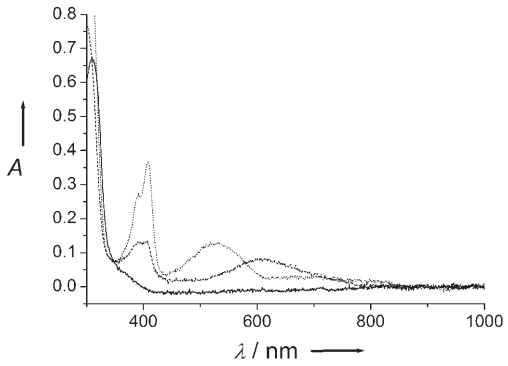

Figure 5. Electronic spectra of 0.05 mM solutions of **3** (solid lines), the electrogenerated $\mathbf{3}^+$ (dashed lines), and $\mathbf{3}^{2+}$ (dotted lines) in CH_2Cl_2 containing 0.005 M TBAP. $T = 233$ K, path length = 1.000 cm.

By contrast, the absorption spectrum dramatically changes when pyridine is added to **2**: the UV/Vis spectral features of **2** progressively disappear and are replaced by a spectrum similar to that of **3** (Figure 6). This indicates that **2** is converted into a high-spin octahedral Ni^{II} complex, $\mathbf{2}_{Py}$, because of the axial coordination of two pyridine molecules to the initial square-planar nickel ion. A $\log\beta_1$ value of 1.4 ± 0.1 was obtained at 298 K for the equilibrium described by Equation (1).

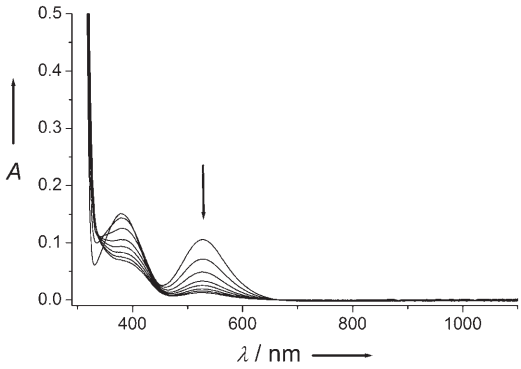

Figure 6. Titration of a 0.05 mM CH_2Cl_2 solution of **2** with 0→7000 equivalents of pyridine (conversion of **2** into $\mathbf{2}_{Py}$). The arrow indicates the direction of spectral change. $T = 298$ K, path length = 1.000 cm.

$$\mathbf{2} + 2\,Py \rightleftharpoons \mathbf{2}_{Py} \qquad \beta_1 = [\mathbf{2}_{Py}]/([\mathbf{2}] \times [Py]^2) \qquad (1)$$

Complexes **1** and **2** thus consist of square-planar d^8 low-spin Ni^{II} complexes, while **3** comprises an octahedral d^8 high-spin Ni^{II}. In the presence of exogenous pyridine, the metal centers of **1** and **3** retain their spin configuration. This is not the case for **2**, as it is converted into $\mathbf{2}_{Py}$, an octahedral d^8 high-spin Ni^{II} complex with two pyridines occupying the apical positions. As **2** alone exhibits the spin transition in the presence of pyridine, the hybridization of the coordinating nitrogen atoms appears to be crucial in conferring such properties on square-planar Ni^{II} complexes.

Electrochemistry of the Ni^{II} complexes: The electrochemical behavior of millimolar solutions of the nickel complexes **1**–**3** in the presence or absence of added pyridine was investigated by cyclic voltammetry (CV) of electrolytic solutions in CH_2Cl_2 with 0.1 M TBAP. All potentials are referenced versus the ferrocenium/ferrocene couple, which was used as an internal standard.

The CV curves of **1** and **3** (Figure 7, Table 4) display two successive reversible redox waves at $E_{1/2}{}^1 = 0.586$ and $E_{1/2}{}^2 = 1.046$ V for **1** and at $E_{1/2}{}^1 = 0.094$ and $E_{1/2}{}^2 = 0.358$ V for **3**.

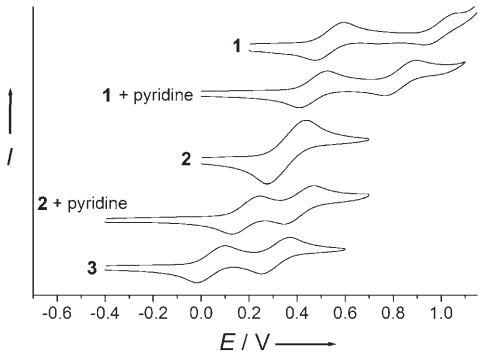

Figure 7. CV curves of 1 mM solutions of the complexes **1**–**3** in CH_2Cl_2 containing 0.1 M TBAP. Scan rate: 0.1 $V s^{-1}$, $T = 298$ K. The potentials are referenced versus the Fc^+/Fc couple. For **1**+pyridine and **2**+pyridine, 100 and 200 molar equivalents of pyridine, respectively, were added to the medium.

Table 4. Redox properties of the nickel complexes.

Complex	Solvent	$E_{1/2}$ [V][a]	
1	CH_2Cl_2	0.586	1.046
	CH_2Cl_2+100 equiv of Py	0.518	0.878
2	CH_2Cl_2		0.406[b]
	CH_2Cl_2+200 equiv of Py	0.254	0.462
3	CH_2Cl_2	0.094	0.358

[a] Potential values given versus the Fc/Fc^+ reference electrode, T = 298 K, complex concentrations of 1 mM; $E_{1/2}$ values were obtained from differential pulse voltammetry (DPV) measurements by adding half of the pulse amplitude to the potential peak E_p value. The confidence level is ±0.005 V. [b] Potential corresponding to the two-electron redox process.

Coulometric titrations showed that these correspond to one-electron processes. As will be shown and discussed below, electrochemical oxidation of **1** and **3** is ligand centered and leads successively to the formation of mono- and bisphenoxyl radical species. The large separation between the half-wave potentials for both processes (0.460 and 0.264 V for **1** and **3**, respectively) indicates that oxidation of one phenolate moiety in the complex greatly influences the second one, a result suggesting a possible structural rearrangement of the coordination sphere upon oxidation and the existence of a strong electrochemical communication through bonds and space in these complexes with two chemically equivalent phenolate groups. The half-wave potentials for both processes are found to be higher for **1** than for **3** (Table 4). The $E_{1/2}{}^1$ value for **1** is very close to that reported for the [Ni(L^1)] complex,[9] whose structure differs from that of **1** only in the spacer, which is an *o*-phenylene diamine in [Ni(L^1)] and an ethylene diimine in **1**. Weaker electrochemical communication, and structural rearrangement, due to the rigid spacer of [Ni(L^1)] results in an $E_{1/2}{}^2$ value which is approximately 0.2 V lower for [Ni(L^1)] than for **1**.[9]

The CV curve of **2** exhibits a single reversible two-electron wave (Figure 7), as judged from coulometric titration, with the formation of a bisphenoxyl radical, $\mathbf{2}^{2+}$ (see below). The chemically equivalent phenolate units linked by an ethylene diamine spacer are thus noninteracting in **2**. For molecules bearing two fully noninteracting, chemically equivalent, redox-active subunits, the difference in potential between the first and the second electron transfer is close to 36 mV; this leads to a CV curve displaying the shape of that for a one-electron transfer but with a peak current twice as large.[17]

In the presence of 100 equivalents of pyridine, the two reversible redox waves of **1** are negatively shifted ($\Delta E_{1/2}{}^1 = -68$ mV, $\Delta E_{1/2}{}^2 = -168$ mV), a result showing that the oxidized forms are stabilized in the presence of additional exogenous N-donor ligands (Figure 7).

The CV curve of **2** in the presence of 200 equivalents of pyridine, thereby allowing the conversion of more than 80% of **2** into $\mathbf{2_{Py}}$, contrasts greatly with that obtained in pure electrolyte: the new curve exhibits two reversible one-electron redox waves (Figure 7) at $E_{1/2}{}^1 = 0.254$ V and $E_{1/2}{}^2 = 0.462$ V, respectively. The electrochemical features of $\mathbf{2_{Py}}$ are intermediate between those of **3** and **1**+pyridine. The $E_{1/2}{}^1$ and $E_{1/2}{}^2$ values of **2** are higher than those of **3**. Stabilization of the oxidized forms of **2** with two exogenous coordinating pyridines is thus weaker than that observed with **3**, which bears two endogenous coordinating pyridines in a templating framework.

The electrochemical behavior of these complexes is thus dictated by the electrochemical communication through space and bonds between the two phenolate subunits and by the stabilization of the oxidized forms in the six-coordinate complexes.

For each complex, a controlled potential electrolysis was performed at 238 K under bubbling argon, at a carbon-felt working electrode, in order to generate the one-electron-oxidized (E applied slightly higher than $E_{1/2}{}^1$) and doubly oxidized (E applied slightly higher than $E_{1/2}{}^2$) products. Rotating-disc electrode (RDE) voltammetry was used to determine the yield of electrogenerated species by comparison between the heights of the initial anodic RDE waves and those of the resulting cathodic RDE waves after consumption of one or two electrons at the appropriate potential. $\mathbf{1}^+$, $\mathbf{2_{Py}}^+$, and $\mathbf{3}^+$ were produced in at least 95% yield, while $\mathbf{2}^{2+}$, $\mathbf{2_{Py}}^{2+}$, and $\mathbf{3}^{2+}$ could be electrogenerated in 90% yield. The maximal yield of $\mathbf{1}^{2+}$ was found to be around 50%, with the final solution consisting of an equimolar mixture of $\mathbf{1}^+$ and $\mathbf{1}^{2+}$. Continuation of the electrolysis on this solution did not afford $\mathbf{1}^{2+}$ in higher yield, with slow decomposition of $\mathbf{1}^{2+}$ being observed instead.

One-electron-oxidized complexes in CH_2Cl_2 and CH_2Cl_2+pyridine: The electronic spectrum of $\mathbf{1}^+$ in CH_2Cl_2 exhibits, in the near-infrared region, remarkably intense bands at 899 ($\varepsilon = 2560$) and 1090 nm (6980 $M^{-1}cm^{-1}$), which correspond to CT transitions (Figure 3, Table 3). Additional features are observed at 379 ($\varepsilon = 8060$), 399 (7340), and 436 nm (shoulder; 4920 $M^{-1}cm^{-1}$), where the typical transitions of phenoxyl radicals are expected to be found.[18] These data thus suggest a significant ligand radical character for $\mathbf{1}^+$. This behavior is close to that observed for $[Ni(L^1)]^+$,[9] thereby showing that the spacer is not of prime importance in dictating the oxidation locus in nickel complexes of salen ligands.

The UV/Vis spectrum of $\mathbf{1}^+$ in the mixture of CH_2Cl_2 and pyridine is dramatically different to that recorded in neat CH_2Cl_2, as the high-intensity near-infrared CT bands are absent (Figure 8). Its electronic spectrum consists of bands

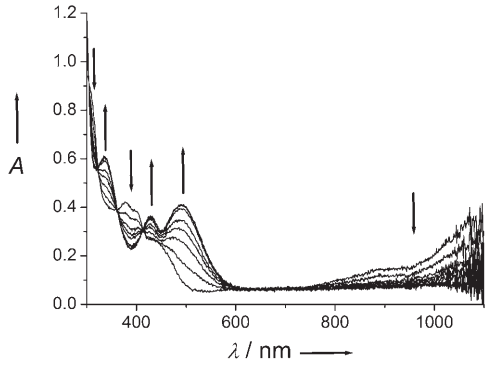

Figure 8. Titration of a 0.05 mM CH_2Cl_2 solution of $\mathbf{1}^+$ with 0→50 equivalents of pyridine (conversion of $\mathbf{1}^+$ into $\mathbf{1_{Py}}^+$). Arrows indicate the spectral changes upon addition of pyridine. $T = 238$ K, path length = 1.000 cm.

at 337 ($\varepsilon = 12140$), 429 (72800), and 493 nm (8140 $M^{-1}cm^{-1}$). Based on the similarities between the spectrum of $\mathbf{1}^+$ in the mixture of CH_2Cl_2 and pyridine and those of octahedral Ni^{III} complexes of Schiff base ligands,[9] the former could be considered as an octahedral Ni^{III} complex with two pyridine molecules axially bonded to the metal ion; it will be denoted $\mathbf{1_{Py}}^+$. The affinity of $\mathbf{1}^+$ for pyridine was obtained from a UV/Vis titration in CH_2Cl_2 at 238 K (Figure 8): Upon addition of pyridine, the spectrum of $\mathbf{1}^+$ disappears and is progressively replaced by that of $\mathbf{1_{Py}}^+$. Isosbestic points could be distinguished at 304, 323, 362, 413, and 640 nm, thereby showing that only two distinct chromophores are in equilibrium. By consideration of Equation (2), a $\log\beta_2$ value of 8.60 ± 0.11 was obtained, which is within the range of that obtained for $[Ni(L^1)]^+$.[9]

$$\mathbf{1}^+ + 2\,Py \rightleftharpoons \mathbf{1_{Py}}^+ \qquad \beta_2 = [\mathbf{1_{Py}}^+]/([\mathbf{1}] \times [Py]^2) \qquad (2)$$

The cation $\mathbf{2}^+$ could not be generated in CH_2Cl_2 (see above) as the chemically equivalent phenolate units are noninteracting and thus electrochemical oxidation directly affords the bisphenoxyl radical species $\mathbf{2}^{2+}$.

The electronic spectra of $\mathbf{2_{Py}}^+$ in CH_2Cl_2 and pyridine and of $\mathbf{3}^+$ in CH_2Cl_2 (or CH_2Cl_2 and pyridine) are very similar, with bands at 391 ($\varepsilon = 3160$), 405 (3140), and 611 nm (broader; 2160 $M^{-1}cm^{-1}$) for $\mathbf{3}^+$ and at 393 ($\varepsilon = 2800$), 412 (3300), and 665 nm (broader; 900 $M^{-1}cm^{-1}$) for $\mathbf{2_{Py}}^+$ (Figure 5, Figure 9, Table 3). These absorptions correspond to the typical π–π* transitions of phenoxyl radicals and thereby indicate that $\mathbf{3}^+$ and $\mathbf{2_{Py}}^+$ are phenoxyl radical complexes.[18]

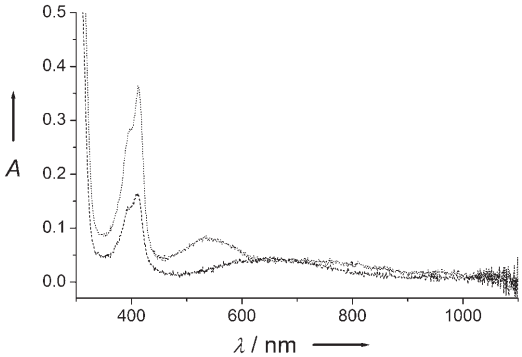

Figure 9. Electronic spectra of 0.05 mM solutions of the electrogenerated $\mathbf{2_{Py}}^+$ (dashed lines) and $\mathbf{2_{Py}}^{2+}$ (dotted lines) in CH_2Cl_2 containing 0.005 M TBAP and 0.2 M pyridine. $T = 233$ K, path length = 1.000 cm.

The X-band EPR spectrum of $\mathbf{1}^+$ (Figure 10a) at 200 K in CH_2Cl_2 (with 0.1 M TBAP) is characterized by an unresolved ($S = {}^1/_2$) signal centered at $g_{iso} = 2.034$ (peak-to-peak line width of 4 mT). This g_{iso} value, intermediate between those

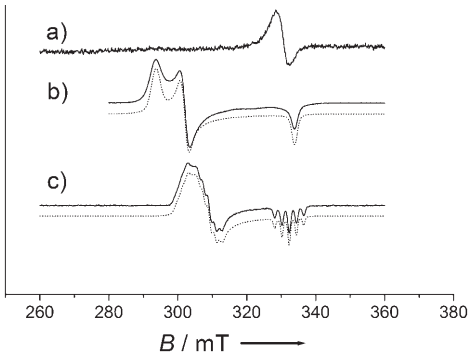

Figure 10. X-band EPR spectra of 1 mM solutions in CH_2Cl_2 containing 0.1 M TBAP of a) $\mathbf{1}^+$ at 260 K, b) $\mathbf{1}^+$ at 4 K, and c) $\mathbf{1}^+$ with 100 equivalents of pyridine at 100 K. Solid lines are experimental spectra, dotted lines represent simulations performed by using the parameters given in the text. a) Microwave frequency 9.42 GHz, power 20 mW, modulation frequency 100 KHz, amplitude 0.099 mT; b) microwave frequency 9.44 GHz, power 1 mW, modulation frequency 100 KHz, amplitude 0.099 mT; c) microwave frequency 9.42 GHz, power 20 mW, modulation frequency 100 KHz, amplitude 0.197 mT.

of zinc(II) complexes incorporating coordinated phenoxyl radicals (lower than 2.01)[19] and those of Ni^{III} complexes (roughly 2.13–2.18),[20] shows that $\mathbf{1}^+$ is best formulated as a ligand radical, with partial delocalization of the unpaired

electron onto the orbitals of the nickel ion.[8] The EPR spectrum of $\mathbf{1}^+$ in CH_2Cl_2 (with 0.1 M TBAP) at 100 K contrasts with that recorded at 200 K, as it consists of a rhombic ($S=^1/_2$) signal (Figure 10b, Table 5), with g values at 2.298, 2.234, and 2.021 ($g_{av}=(2.298+2.234+2.021)/3=2.18$), values that are typical of Ni^{III} complexes in a low-spin configuration. Such behavior has been recently discussed in terms of a valence tautomerism governed by the temperature or relaxation effects.[8,9] The 100 K EPR spectrum of the pyridine adduct $\mathbf{1_{Py}}^+$ in CH_2Cl_2 and pyridine is shown in Figure 10c. A low-spin ($S=^1/_2$) Ni^{III} signal, with hyperfine splitting in each of the three g components, is observed (Table 5). The pattern of g values, g_x (2.221) $\approx$ g_y (2.176) $>$ g_z (2.025) $\approx$ g_e (2.0023), is indicative of a d_z2 ground state where the z axis is perpendicular to the plane of the molecule. In addition, the presence of one well-resolved quintuplet in the high-field component g_z ($A_{2N}=2.10$ mT), as well as two less-resolved quintuplets in the low-field components g_x and g_y ($A_{2N}=1.55$ mT), implies the existence of a six-coordinate Ni^{III} complex $\mathbf{1_{Py}}^+$ with two equivalent pyridines axially bonded. A slight difference in g tensor anisotropy exists between $\mathbf{1_{Py}}^+$ and the pyridine adduct of $[Ni(L^1)]^+$, a fact indicating that the spacer contributes significantly to the electronic distribution in the complex.

Table 5. EPR parameters of the one-electron oxidized nickel complexes.

Complex	Solvent[a]	g values				A values[b]		
		g_{xx}	g_{yy}	g_{zz}	g_{av}	A_{xx}	A_{yy}	A_{zz}
$\mathbf{1}^+$	CH_2Cl_2	2.298	2.234	2.021	2.18	–	–	–
$\mathbf{1_{Py}}^+$	CH_2Cl_2+Py[c]	2.221	2.176	2.025	2.14	1.55	1.55	2.10
$\mathbf{2_{Py}}^+$	CH_2Cl_2+Py[c]		[d]			–	–	–
$\mathbf{3}^+$	CH_2Cl_2	2.22		2.22	–	–	–	

[a] Measured at 100 K, in the presence of 0.1 M TBAP. [b] Corresponds to the interaction of the electronic spin with two equivalent ^{14}N atoms. [c] In the presence of 0.2 M pyridine. [d] $S=^3/_2$ system with a $|D|$ value larger than the X-band microwave quantum: only part of the spectrum could be observed, thereby precluding any accurate determination of g values.

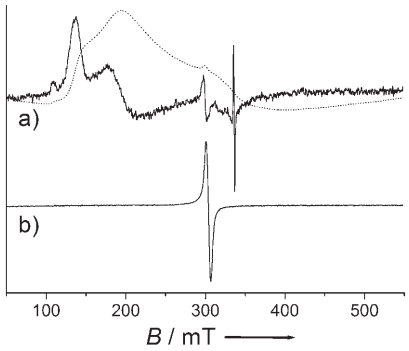

Figure 11. X-band EPR spectra (100 K) of 5 mM solutions in CH_2Cl_2 containing 0.1 M TBAP of a) $\mathbf{2_{Py}}^+$ with 200 equivalents of pyridine (solid lines) and its integrated spectrum (dotted lines) and b) $\mathbf{3}^+$. Microwave frequency 9.42 GHz, power 20 mW, modulation frequency 100 KHz, amplitude a) 0.495 mT, b) 0.197 mT.

The EPR spectrum of $\mathbf{2_{Py}}^+$ in CH_2Cl_2 and pyridine at 100 K is shown in Figure 11a. The narrow signals at $g=2.00$ and $g=2.24$ are due to unknown impurities accounting for less than 2% of the total signal. The major signals at 110, 137, 195, and 315 mT are attributed to an $S=^3/_2$ system with a $|D|$ value larger than the microwave quantum energy (0.3 cm^{-1}), which shows that $\mathbf{2_{Py}}^+$ comprises a phenoxyl radical ferromagnetically coupled to a high-spin Ni^{II} ion (Table 5). Such behavior (large $|D|$ values and ferromagnetic coupling) is commonly encountered in octahedral high-spin Ni^{II} complexes containing a coordinated semiquinone ligand.[6]

The X-band EPR spectrum of $\mathbf{3}^+$ in CH_2Cl_2 at 100 K contrasts sharply with those of $\mathbf{1_{Py}}^+$ and $\mathbf{2_{Py}}^+$ under similar conditions (Figure 11a, Table 5), as it consists of an isotropic signal centered at a g value of 2.22. Its isotropic nature ruled out the existence of a Ni^{III} complex such as that in $\mathbf{1_{Py}}^+$ or a $S=^3/_2$ system similar to $\mathbf{2_{Py}}^+$. This unusual behavior has been recently reported by Yamauchi and co-workers and is interpreted by antiferromagnetic coupling between a phenoxyl radical and a d^8 high-spin Ni^{II}.[11]

The pyridine adduct $\mathbf{1_{Py}}^+$ could thus be formulated as a nickel(III) species, while $\mathbf{2_{Py}}^+$ and $\mathbf{3}^+$ are high-spin Ni^{II} complexes containing a coordinated phenoxyl radical. These results show that pyridine axial ligation promotes an electron transfer from the metal to the ligand in $\mathbf{1_{Py}}^+$. Moreover, it has been previously shown in related free ligands that changes in the hybridization of the nitrogen atoms strongly affect the oxidation potential of phenol. A double effect (ligand field combined with changes in the electrochemical properties of the phenol) is thus proposed to explain the dramatically different behavior observed with $\mathbf{1_{Py}}^+$ and $\mathbf{2_{Py}}^+$. The initial metal spin configuration, d^8 low-spin Ni^{II} ion for **1** or d^8 high-spin Ni^{II} ion for **3**, may also contribute to this difference, as it is correlated to the energy of the potentially redox-active orbital on the metal. In addition, the magnetic interaction between the metal and the radical is strongly affected by the nature of the pyridine, that is, whether it is endogenous or exogenous from the ligand. Pyridine is expected to bind the metal ion more strongly in **3** than in $\mathbf{2_{Py}}^+$ (chelate effect), which would result in some geometrical changes, as reflected by shifts in the $E_{1/2}$ values. This may affect the overlap between the nickel and phenoxyl orbitals and thus the magnetic coupling.

Two-electron-oxidized complexes in CH_2Cl_2 and CH_2Cl_2+pyridine: The electronic spectrum of $\mathbf{1}^{2+}$ in CH_2Cl_2 has been calculated by subtracting the electronic spectrum of $\mathbf{1}^+$ from the electronic spectrum of the electrolyzed solution and assuming the formation of an equimolar mixture of $\mathbf{1}^{2+}$ and $\mathbf{1}^+$ (see above). The calculated spectrum exhibits strong absorption bands at 395 ($\varepsilon=5260$) and 414 nm (6230 $M^{-1}cm^{-1}$), as well as a broad band at 550 nm ($\varepsilon \approx 1000$ $M^{-1}cm^{-1}$; Figure 3, Table 3). No high-intensity CT transition could be detected in the 800–1100 nm region. The other two-electron-oxidized complexes exhibit roughly similar absorption bands. For $\mathbf{2}^{2+}$ in CH_2Cl_2, bands were ob-

served at 390 ($\varepsilon = 5740$), 406 (7700), and 530 nm (broad; 1960 $M^{-1}cm^{-1}$). $\mathbf{2_{Py}}^{2+}$ in CH_2Cl_2 and pyridine exhibted bands at 397 ($\varepsilon = 5700$), 411 (7300), and 540 nm (broad; 1580 $M^{-1}cm^{-1}$). For $\mathbf{3}^{2+}$ in CH_2Cl_2, bands appeared at 391 ($\varepsilon = 6400$), 408 (8240), and 528 nm (3460 $M^{-1}cm^{-1}$; Figure 4, Figure 5, Figure 9, Table 3).

These bands match well the π–π* transitions of the monophenoxyl radical complexes $\mathbf{2_{Py}}^{+}$ and $\mathbf{3}^{+}$. They are twice as large in the dications, which suggests that these species are Ni^{II} bisphenoxyl radical complexes. This assumption is corroborated by the close similarity of these UV/Vis data with those of the copper(II) bisphenoxyl radical complex of the reduced Jacobsen ligand described by Pratt and Stack (405 ($\varepsilon = 5800$), 418 (5800), and 592 nm (1300 $M^{-1}cm^{-1}$)).[4]

The two-electron oxidized species $\mathbf{1}^{2+}$, $\mathbf{2}^{2+}$, $\mathbf{2_{Py}}^{2+}$, and $\mathbf{3}^{2+}$ were found to be X-band EPR silent at 100 K. The state populated at 100 K is thus either diamagnetic ($S = 0$) or paramagnetic ($S = 1$) with large zero-field splitting parameters. This unambiguously gives evidence for a magnetic interaction between the radical spins.

The dications $\mathbf{1}^{2+}$, $\mathbf{2}^{2+}$, $\mathbf{2_{Py}}^{2+}$, and $\mathbf{3}^{2+}$ are thus bisphenoxyl radical species in which the two phenoxyl moieties and the nickel ion are magnetically interacting.

to-high-spin transition promoted by the addition of pyridine to square-planar Ni^{II} complexes. The chemically induced spin transition is possible only when the coordinating nitrogen atoms are amino (**2**), and not imino (as in **1**), ones.

Hybridization not only controls the spin state of the metal center but also the oxidation locus (Scheme 2), which is

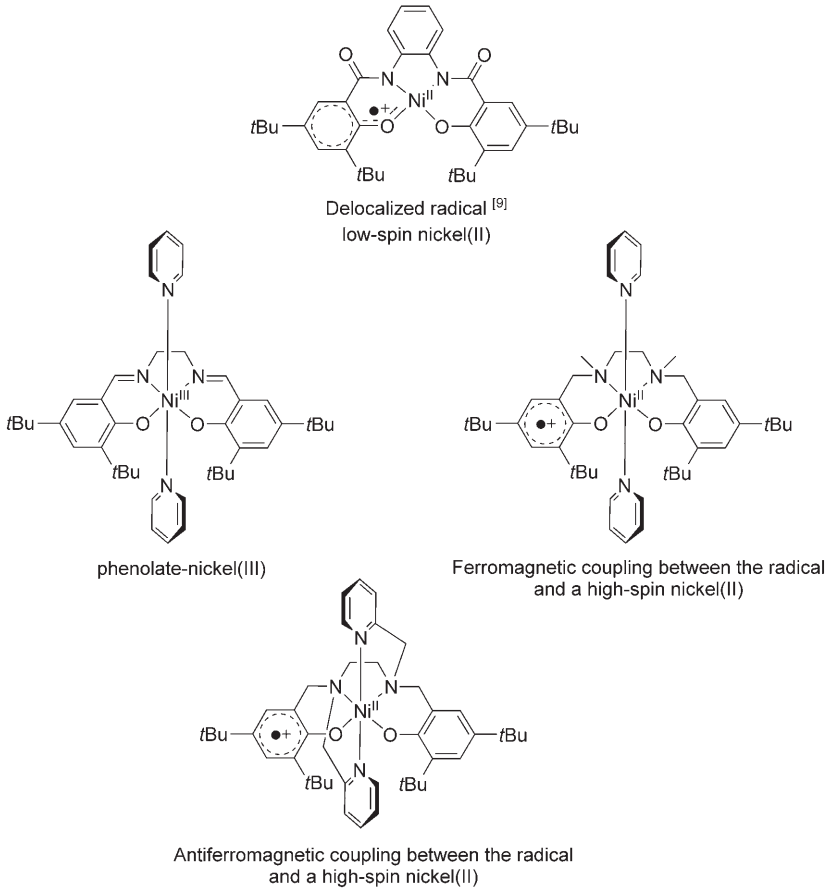

Scheme 2. Modulation of the oxidation locus by the ligand field and coordination of pyridine.

Conclusion

Complex **1** comprises a low-spin Ni^{II} ion, as is usually observed in square-planar Ni^{II} complexes of salen-type ligands. Its one-electron-oxidation product, in the presence of pyridine, is a six-coordinate Ni^{III} complex, $\mathbf{1_{Py}}^{+}$, which has two equivalent axially bonded pyridines.

Coordination changes around an Ni^{II} ion, from square planar to octahedral, are susceptible to promote a low-to-high-spin transition at the metal center. In the one-electron-oxidized octahedral nickel complexes of salen-type ligands, there is therefore a subtle balance that affords either a high-spin Ni^{II} radical or a nickel(III) species (valence tautomerism).

We show here that hybridization of the coordinating nitrogen atoms is of prime importance in controlling the low-either metal-centered with imines ($\mathbf{1_{Py}}^{+}$) or ligand-centered with amines ($\mathbf{2_{Py}}^{+}$, $\mathbf{3}^{+}$). Control of the magnetic interaction between the radical and the Ni^{II} spins has also been achieved. By incorporation of the axial pyridines in the ligand structure ($\mathbf{2_{Py}}^{+}$), an $S = {}^{3}/_{2}$ species is obtained, while a $S = {}^{1}/_{2}$ system is obtained when these pyridines come from the solvent (as in $\mathbf{3}^{+}$).

Finally two-electron oxidation of all the Ni^{II} complexes affords bisphenoxyl radical species, irrespective of the hybridization of the nitrogen atoms.

These results show how fascinating the oxidative chemistry of nickel phenolate systems is. They illustrate the high level of control that can be achieved for both the nickel spin state, and the oxidation locus, simply by changing the hybridization of the coordinating nitrogen atoms in salen-type ligands.

Experimental Section

General: All chemicals were of reagent grade and used without further purification. NMR spectra (^{1}H at 300 MHz and ^{13}C at 75 MHz) were recorded on a Bruker AM 300 spectrometer. Chemical shifts are given relative to tetramethylsilane (TMS). Mass spectra were recorded on a Thermofunnigen (EI/DCI) apparatus.

UV/Vis spectroscopy: UV/Vis spectra (298 K) were recorded on a Perkin–Elmer Lambda 2 spectrophotometer equipped with a temperature-controller unit set at 298 K. The pathlength of the quartz cell was 1.000 cm. UV/Vis spectra (238 K) were recorded on a Cary 50 spectrophotometer equipped with a Hellma low-temperature immersion probe (quartz cell with 1.000 cm pathlength). The temperature was controlled with a Lauda RK8 KS cryostat. The affinity constants were obtained from refinement of the UV/Vis titration data of the complexes with pyridine in CH_2Cl_2. Fitting was performed with the commercial Specfit 3.0.37 software (Spectrum Software Associates).

EPR spectroscopy: X-band EPR spectra were recorded on a Bruker ESP 300E spectrometer equipped with a Bruker nitrogen-flow cryostat. Spectra were treated by using the WINEPR software and simulated by using the Bruker Simfonia software. Spectra at 100 K were recorded on 200-μL samples, while variable-temperature experiments were performed on 50-μL samples.

Electrochemistry: Cyclic voltammetry, rotating-disc electrode voltammetry, and differential pulse voltammetry experiments were carried out at 298 K in millimolar solutions of the complexes in CH_2Cl_2 containing TBAP as a supporting electrolyte, with a CHI 660 potentiostat and a conventional three-electrode electrochemical cell. A glassy carbon disc was used as the working electrode (3 mm in diameter) and a Pt wire was the secondary electrode. The reference electrode consisted of the 0.01 M $Ag/AgNO_3$ system. The potential of the regular ferrocenium/ferrocene (Fc^+/Fc) couple, used as an internal reference, is +0.087 V under our experimental conditions. Experiments were performed under an argon atmosphere. Electrolysis at a carbon-felt electrode ($1\times1\times0.5$ cm) was performed at 233 K, by controlled-potential electrolysis, with a PAR 273 potentiostat.

Crystal structure analysis: For all structures, collected reflections were corrected for Lorentz and polarization effects but not for absorption. The structures were solved by direct methods and refined by using the Texsan software. All non-hydrogen atoms were refined with anisotropic thermal parameters. Hydrogen atoms were generated in idealized positions, riding on the carrier atoms, with isotropic thermal parameters. CCDC-296376 and CCDC-296377 contain the supplementary crystallographic data for this paper (for **2** and **3**, respectively). These data can be obtained free of charge from the Cambridge Crystallographic Data Centre via www.ccdc.cam.ac.uk/data_request/cif.

Preparation of the ligands and complexes: The ligands H_2L, H_2L^{Me}, and H_2L^{Py} have been described previously.[5,12,13]

1: H_2L (100 mg, 0.20 mmol) and $Ni(ClO_4)_2\cdot6H_2O$ (74 mg, 0.20 mmol) were dissolved in MeOH (30 mL) in the presence of NEt_3 (56 μL, 2 equiv) and the solution was stirred for 1 day. A dark brown precipitate of **1** (83 mg, 76%) was then collected. elemental analysis calcd (%) for $C_{32}H_{46}N_2O_2Ni$: C 69.96, H 8.44, N 5.10; found: C 70.03, H 8.45, N 5.11; ^{1}H NMR (300 MHz, CD_2Cl_2, 298 K, TMS): $\delta=7.44$ (s, 2H), 7.22 (d, $^4J=2.5$ Hz, 2H), 6.84 (d, $^4J=2.5$ Hz, 2H), 3.24 (s, 4H), 1.29 (s, 18H), 1.19 ppm (s, 18H); UV/Vis (CH_2Cl_2, 238 K): λ_{max} (ε) = 349 (9180), 422 (7380), 449 nm (4740 $M^{-1}cm^{-1}$); IR (neat): $\tilde{\nu}=2946$, 2903, 2867 (w, ν_{CH}), 1624 (s, $\nu_{C=C}$), 1434 (s, ν_{CH_2}) and 1317 cm^{-1} (s, ν_{C-O}); MS: *m*/*z* (%): 549 (100) $[M+H]^+$.

2: NEt_3 (54 μL, 2 equiv) was added to a solution of H_2L^{Me} (100 mg, 0.19 mmol) in MeOH (20 mL). This was followed by addition of a solution of $Ni(OAc)_2\cdot4H_2O$ (48 mg, 0.19 mmol) in MeOH (20 mL). The mixture was refluxed for three hours and the formation of **2** as a pink precipitate was observed. After cooling of the reaction mixture to 298 K, the complex was isolated by filtration (68 mg, 63%). Crystals were obtained from the filtrate by slow evaporation of MeOH. Elemental analysis calcd (%) for $C_{34}H_{54}N_2O_2Ni$: C 70.23, H 9.36, N 4.82; found: C 69.98, H 9.37, N 54.79; ^{1}H NMR (300 MHz, CD_2Cl_2, 298 K, TMS): $\delta=7.32$ (s, 2H), 6.73 (s, 2H), 3.65 (brs, 4H), 2.25 (brs, 4H), 1.38 (s, 18H), 1.25 ppm (s, 18H); UV/Vis (CH_2Cl_2, 238 K): λ_{max} (ε) = 311 (10540), 377 (2320), 522 nm (1960 $M^{-1}cm^{-1}$); IR (neat): $\tilde{\nu}=2945$, 2898, 2859 (w, ν_{CH}), 1612 (s, $\nu_{C=C}$), 1472 (s, ν_{CH_2}), 1305 cm^{-1} (s, ν_{C-O}); MS: *m*/*z* (%): 581 (100) $[M+H]^+$.

3: A solution of $Ni(OAc)_2\cdot4H_2O$ (36 mg, 0.15 mmol) in MeOH (20 mL) was added to a solution of H_2L^{Py} (100 mg, 0.15 mmol) and NEt_3 (40 μL, 2 equiv) in MeOH (20 mL). After three hours of reflux and evaporation of two thirds of the solvent, product **3** crystallized at −20 °C overnight and was isolated by filtration (59 mg, 53%). Elemental analysis calcd (%) for $C_{44}H_{60}N_4O_2Ni$: C 71.84, H 8.23, N 7.62; found: C 72.15, H 8.25, N 7.69; ^{1}H NMR (300 MHz, $CDCl_3$, 298 K, TMS): $\delta=77.21$ (brs, 2H), 67.36 (brs,2H), 53.37 (brs, 2H), 44.54 (s, 4H), 36.33 (s, 4H), 27.55 (s, 4H), 10.39 (s, 4H), 1.05 ppm (s, 36H); UV/Vis (CH_2Cl_2, 238 K): λ_{max} (ε) = 310 (13500), 369 nm (760 $M^{-1}cm^{-1}$); IR (neat): $\tilde{\nu}=2940$, 2889 (w, ν_{CH}), 1600 (s, $\nu_{C=C}$), 1460 (s, ν_{CH_2}), 1321 cm^{-1} (s, ν_{C-O}); MS: *m*/*z* (%): 735 (100) $[M+H]^+$.

[1] J. Stubbe, W. A. van der Donk, *Chem. Rev.* **1998**, *98*, 705–762; M. Fontecave, J.-L. Pierre, *C. R. Acad. Sci. Paris, Chimie* **2001**, *4*, 531–538; W. Kaim, *Dalton Trans.* **2003**, 761–768.

[2] G. Avigad, D. Amaral, C. Asensio, B. L. Horecker, *J. Biol. Chem.* **1962**, *237*, 2736–2743; M. M. Whittaker, J. W. Whittaker, *J. Biol. Chem.* **1988**, *263*, 6074–6080; M. M. Whittaker, J. W. Whittaker, *J. Biol. Chem.* **1990**, *265*, 9610–9613; N. Ito, S. E. V. Phillips, C. Stevens, Z. B. Ogel, M. J. McPherson, J. N. Keen, K. D. S. Yadav, P. J. Knowles, *Nature* **1991**, *350*, 87–90; G. T. Babcock, M. K. El-Deeb, P. O. Sandusky, M. M. Whittaker, J. W. Whittaker, *J. Am. Chem. Soc.* **1992**, *114*, 3727–3734; N. Ito, S. E. V. Phillips, K. D. S. Yadav, P. F. Knowles, *J. Mol. Biol.* **1994**, *238*, 794–814; J. W. Whittaker in *Metal Ions in Biological Systems, Vol. 30* (Eds.: H. Sigel, A. Sigel), Marcel Dekker, New York, **1994**, pp. 315–360; J. W. Whittaker in *Advances in Protein Chemistry, Vol. 60* (Eds.: A. Richards, E. B. Graller), Elsevier, New York, **2002**, pp. 1–49; J. W. Whittaker, *Chem. Rev.* **2003**, *103*, 2347–2364; M. S. Rogers, D. M. Dooley, *Curr. Opin. Chem. Biol.* **2003**, *7*, 189–196.

[3] For recent papers, see: B. A. Jazdzewski, A. M. Reynolds, P. L. Holland, V. G. Young, Jr., S. Kaderli, A. D. Zuberbühler, W. B. Tolman, *J. Biol. Inorg. Chem.* **2003**, *8*, 381–393; M. Vaidyanathan, M. Palaniandavar, R. S. Gopalan, *Ind. J. Chem.* **2003**, *42A*, 2210–2222; G. Klein, J. M. Robertus, M. Watanabee, R. C. Pratt, T. D. P. Stack, *Chem. Commun.* **2003**, 630–631; A. Philibert, F. Thomas, C. Philouze, S. Hamman, E. Saint-Aman, J.-L. Pierre, *Chem. Eur. J.* **2003**, *9*, 3803–3812; A. Neves, A. dos Anjos, A. J. Bortoluzzi, B. Szpoganicz, E. W. Schwingel, A. S. Mangrich, *Inorg. Chim. Acta* **2003**, *356*, 41–50; O. Seneque, M. Campion, B. Douziech, M. Giorgi, Y. Le Mest, O. Reinaud, *Dalton Trans.* **2003**, 4216–4218; R. C. Pratt, T. D. P. Stack, *Inorg. Chem.* **2004**, *43*, 8030–8040; F. Michel, F. Thomas, S. Hamman, E. Saint-Aman, J.-L. Pierre, *Chem. Eur. J.* **2004**, *10*, 4115–4125; M. Taki, H. Hattori, T. Osako, S. Nagatomo, M. Shiro, T. Kitagawa, S. Itoh, *Inorg. Chim. Acta* **2004**, *357*, 3369–3381; T. K. Paine, T. Weyhermüller, K. Wieghardt, P. Chaudhuri, *Dalton Trans.* **2004**, 2092–2101; F. Michel, S. Torelli, F. Thomas, C. Duboc, C. Philouze, C. Belle, S. Hamman, E. Saint-Aman, J.-L. Pierre, *Angew. Chem.* **2005**, *117*, 442–445; *Angew. Chem. Int. Ed.* **2005**, *44*, 438–441; P. Chaudhuri, K. Wieghardt, T. Weyhermüller, T. K. Paine, S. Mukherjee, C. Mukherjee, *Biol. Chem.* **2005**, *386*, 1023–1033; A. Dos Anjos, A. J. Bortoluzzi, R. E. H. M. B. Osorio, R. A. Peralta, G. R. Friedermann, A. S. Mangrich, A. Neves, *Inorg. Chem. Commun.* **2005**, *8*, 249–253; E. Zueva, P. H. Walton, J. E. McGrady, *Dalton Trans.* **2006**, 159–167; A. K. Nairn, S. J. Archibald, R. Bhalla, B. C. Gilbert, E. J. MacLean, S. J. Teat, P. H. Walton, *Dalton Trans.* **2006**, 172–176.

[4] R. C. Pratt, T. D. P. Stack, *J. Am. Chem. Soc.* **2003**, *125*, 8716–8717.

[5] F. Thomas, O. Jarjayes, C. Duboc, C. Philouze, E. Saint-Aman, J.-L. Pierre, *Dalton Trans.* **2004**, 2662–2669.

[6] C. L. Simpson, S. R. Boone, C. G. Pierpont, *Inorg. Chem.* **1989**, *28*, 4379–4385; C. W. Lange, C. G. Pierpont, *Inorg. Chim. Acta* **1997**,

263, 219–224; D. Coucouvanis, S. G. Jonasdottir, D. Christodoulou, C. G. Kim, J. W. Kampf, *Inorg. Chem.* **1993**, *32*, 2987–2988; C. G. Pierpont, *Coord. Chem. Rev.* **2001**, *216–217*, 99–125; A. Caneschi, A. Dei, C. P. Mussari, D. A. Schulz, L. Sorace, K. E. Vostrikova, *Inorg. Chem.* **2002**, *41*, 1086–1092; A. Bencini, C. Carbonera, A. Dei, M. G. F. Vaz, *Dalton Trans.* **2003**, 1701–1706; K. A. Kozhanov, M. P. Bubnov, V. K. Cherkasov, G. K. Fukin, G. A. Abakumov, *Chem. Commun.* **2003**, 2610–2611; C.-H. Sieh, I.-J. Hsu, C.-H. Lee, S.-C. Ke, T. Wang, G.-H. Lee, Y. Wang, J.-M. Chen, J.-F. Lee, W. F. Lians, *Inorg. Chem.* **2003**, *42*, 3925–3933; D. Herebian, F. Neese, K. E. Wieghardt, *J. Am. Chem. Soc.* **2003**, *125*, 10997–11005; M. S. Min, T. Weyhermüller, E. Bothe, K. Wieghardt, *Inorg. Chem.* **2004**, *43*, 2922–2931; H. Ohtsu, K. Tanaka, *Angew. Chem.* **2004**, *116*, 6461–6463; *Angew. Chem. Int. Ed.* **2004**, *43*, 6301–6303; H. Ohtsu, K. Tanaka, *Chem. Eur. J.* **2005**, *11*, 3420–3426.

[7] A. Aukauloo, X. Ottenwaelder, R. Ruiz, S. Poussereau, Y. Pei, Y. Journaux, P. Fleurat, F. Volatron, B. Cervera, M. C. Muñoz, *Eur. J. Inorg. Chem.* **1999**, 1067–1071; D. Herebian, E. Bothe, E. Bill, T. Weyhermüller, K. Wieghardt, *J. Am. Chem. Soc.* **2001**, *123*, 10012–10023; X. Ottenwaelder, R. Ruiz-Garcia, G. Blondin, R. Carasco, J. Cano, D. Lexa, Y. Journaux, A. Aukauloo, *Chem. Commun.* **2004**, 504–505; S. Blanchard, F. Neese, E. Bothe, E. Bill, T. Weyhermüller, K. Wieghardt, *Inorg. Chem.* **2005**, *44*, 3636–3656.

[8] Y. Shimazaki, F. Tani, K. Fului, Y. Naruta, O. Yamauchi, *J. Am. Chem. Soc.* **2003**, *125*, 10512–10513.

[9] O. Rotthaus, O. Jarjayes, F. Thomas, C. Philouze, C. Perez Del Vallee, E. Saint-Aman, J.-L. Pierre, *Chem. Eur. J.* **2006**, *12*, 2293.

[10] J. Müller, A. Kikuchi, E. Bill, T. Weyhermüller, P. Hildebrandt, L. Ould-Moussa, K. Wieghardt, *Inorg. Chim. Acta* **2000**, *297*, 265–277.

[11] Y. Shimazaki, S. Huth, S. Karasawa, S. Hirota, Y. Naruta, O. Yamauchi, *Inorg. Chem.* **2004**, *43*, 7816–7822.

[12] A. Dos Anjos, A. J. Bortoluzzi, B. Szpoganicz, M. S. B. Caro, G. R. Friedermann, A. S. Mangrich, A. Neves, *Inorg. Chim. Acta* **2005**, 3106–3114.

[13] E. Y. Tshuva, I. Goldberg, M. Kol, *J. Am. Chem. Soc.* **2000**, *122*, 10706–10707.

[14] J. Krzystek, J.-H. Park, M. W. Meisel, M. A. Hitchman, H. Stratemeier, L.-C. Brunel, J. Telser, *Inorg. Chem.* **2002**, *41*, 4478–4487; G. Rogez, J.-N. Rebilly, A.-L. Barra, L. Sorace, G. Blondin, N. Kirchner, M. Duran, J. Van Slageren, S. Parsons, L. Ricard, A. Marvilliers, T. Mallah, *Angew. Chem.* **2005**, *117*, 1910–1913; *Angew. Chem. Int. Ed.* **2005**, *44*, 1876–1879.

[15] A. Böttcher, H. Elias, E.-G. Jäger, H. Langfelderova, M. Mazur, L. Müller, H. Paulus, P. Pelikan, M. Rudolph, M. Valko, *Inorg. Chem.* **1993**, *32*, 4131–4138.

[16] S. Mukhopadhyay, D. Mandal, D. Ghosh, I. Goldberg, M. Chaudhury, *Inorg. Chem.* **2003**, *42*, 8439–8445; H. Ohtsu, K. Tanaka, *Inorg. Chem.* **2004**, *43*, 3024–3030.

[17] J. B. Flanagan, S. Margel, A. J. Bard, F. C. Anson, *J. Am. Chem. Soc.* **1978**, *100*, 4248–4253.

[18] R. Liu, K. Morokuma, A. M. Mebel, M. C. Lin, *J. Phys. Chem.* **1996**, *100*, 9314–9322; H. M. Chang, H. H. Jaffe, *Chem. Phys. Lett.* **1973**, *23*, 146–148; H. M. Chang, H. H. Jaffe, C. A. Masmandis, *J. Phys. Chem.* **1975**, *79*, 1118–1129; L. J. Johnston, N. Mathivanan, F. Negri, W. Siebrand, F. Zerbetto, *Can. J. Chem.* **1993**, *71*, 1655–1662; J. Takahashi, T. Shida, *Bull. Chem. Soc. Jpn.* **1994**, *67*, 2038–2046; J. Takahashi, T. Momose, T. Shida, *Bull. Chem. Soc. Jpn.* **1994**, *67*, 964–977; J. G. Radziszewski, M. Gil, A. Gorski, J. Spanget-Larsen, J. Waluk, B. J. Mroz, *J. Chem. Phys.* **2001**, *115*, 9733–9738.

[19] A. Sokolowski, J. Müller, T. Weyhermüller, R. Schnepf, P. Hildebrandt, K. Hildenbrand, E. Bothe, K. Wieghardt, *J. Am. Chem. Soc.* **1997**, *119*, 8889–8900.

[20] R. S. Drago, E. I. Baucom, *Inorg. Chem.* **1972**, *11*, 2064–2069; F. V. Lovecchio, E. S. Gore, D. H. Busch, *J. Am. Chem. Soc.* **1974**, *96*, 3109–3118; H. J. Krüger, R. H. Holm, *Inorg. Chem.* **1987**, *26*, 3645–3647; T. J. Collins, T. R. Nichols, E. S. Uffelman, *J. Am. Chem. Soc.* **1991**, *113*, 4708–4709; F. Azevedo, M. A. Carrondo, B. Castro, M. Convery, D. Domingues, C. Freire, M. T. Duarte, K. Nielsen, I. C. Santos, *Inorg. Chim. Acta* **1994**, *219*, 43–54; D. Pinho, P. Gomes, C. Freire, B. De Castro, *Eur. J. Inorg. Chem.* **2001**, 1483–1493; Z. Xiao, B. O. Patrick, D. Dolphin, *Inorg. Chem.* **2003**, *42*, 8125–8127.

Received: February 23, 2006
Published online: June 29, 2006

